Ab initio random-phase-approximation calculation of the frequency-dependent effective interaction between 3d electrons: Ni, Fe, and MnO

2000 J. Phys.: Condens. Matter 12 2413

(http://iopscience.iop.org/0953-8984/12/11/307)

J. Phys.: Condens. Matter **12** (2000) 2413–2422. Printed in the UK PII: S0953-8984(00)08025-5

Ab initio random-phase-approximation calculation of the frequency-dependent effective interaction between 3d electrons: Ni, Fe, and MnO

Takao Kotani
Department of Physics, Osaka University, Toyonaka 560-0043, Japan

Received 21 September 1999, in final form 7 January 2000

Abstract. We calculate the frequency-dependent effective interaction between 3d electrons for Fe, Ni, and MnO (antiferromagnetic type II) in the random-phase approximation (RPA), where the contributions of 3d electrons to the dielectric function are projected out. It is concluded that the real part of the interaction for Fe and Ni shows only a weak frequency dependence.

1. Introduction

For strongly correlated systems like transition-metal compounds with 3d electrons, the ordinary *ab initio* calculation, which is based on the density-functional (DF) formalism in the local density approximation (LDA), sometimes fails to predict such physical properties as the ground-state magnetism. In such cases, one of the most popular theoretical approaches is based on models such as the Hubbard Hamiltonian, where the effective screened Coulomb interaction acts only between localized electrons, e.g., 3d or 4f electrons. The interaction in these models should be renormalized in the sense that the screenings by other degrees of freedom, typically that of the sp electrons, are taken into account. The screened interactions have also been used in the calculation of the local part of the self-energies in various recently developed methods based on *ab initio* calculations, e.g., T-matrix approaches [1], Igarashi's three-particle approaches [2, 3], and the LDA + U method [4]. A common question in these approaches is that of how to determine the effective interaction.

To date, two different kinds of *ab initio* approach have been proposed. One is the constrained LDA approach [5]; the other is based on the linearized time-dependent Hartree approximation or, equivalently, the random-phase approximation (RPA) [6]. The latter approach was implemented by Springer and Aryasetiawan [7] by using the LMTO (linearized muffin-tin orbital) method and the atomic sphere approximation (ASA). They presented the diagonal part of the interaction calculated by means of the RPA. This method has some advantages over the constrained LDA calculation:

(1) it can give the energy dependence of the interaction;
(2) it can include the non-spherical density response;
(3) all of the components of the interaction matrix are given simultaneously.

These features are not readily available in the constrained method. In this paper, we calculate the energy dependence of all the matrix elements, which are compactly described by the use of three Racah parameters (A, B, and C). We exploit a kind of RPA method to calculate the

0953-8984/00/112413+10$30.00

Racah parameters. In this method (hereafter called the projected RPA (PRPA) method), we use polarization functions from which the contributions of the 3d electrons are projected out. The effective interaction so defined enables us to calculate a self-energy and other quantities, without having to be concerned about the double counting of the effects of polarization arising in the 3d electrons, which otherwise has to be subtracted consistently. This last point is crucial in obtaining the interaction to be used in the various model Hamiltonians. We show that the real part of the calculated interaction for Fe and Ni gives a rather weak frequency dependence after the 3d contributions are projected out.

These calculations are performed on periodic lattices with the usual primitive unit cells. In other words, we assume that the off-site 3d electrons do not contribute much to the screened interaction. In order to confirm the validity of this seemingly crude approximation, we also repeat the calculations with a large unit cell. In this way, we can properly include the contributions of the off-site 3d electrons to the screening. However, we will show that the results are not very different from those obtained by using the ordinary method for the primitive unit cell.

We have tried to apply the PRPA to MnO (antiferromagnetic type II) to calculate the Racah parameters for the Mn 3d basis. However, our analysis shows that the Mn 3d radial functions change rapidly with energy where the projected density of states (PDOS) of Mn 3d is to be calculated. As a result, the Racah parameters are strongly dependent on the choice of the energy $\epsilon_{\mathrm{Mn\,3d}}$ of the radial wave functions which we use for the calculation of the matrix elements. For this reason, we will give Racah parameters calculated by the use of $\epsilon_{\mathrm{Mn\,3d}}$-energies corresponding to (i) occupied and (ii) unoccupied states.

In the LMTO-ASA method, the Kohn–Sham eigenfunctions $\psi^{kj}(\boldsymbol{r}, R)$ are written as linear combinations of the localized MT orbitals (MTOs). Here R is the index for the atomic sphere (AS) and $\boldsymbol{r} = (r, \theta, \phi)$ is a vector denoting the position in each AS ($0 \leqslant r \leqslant \bar{R}$). The MTOs are constructed as linear combinations of the two kinds of on-site basis function. The basis functions are the ϕ-basis and the $\dot{\phi}$-basis, which are written as $\phi_{Rl}(r)Y_L(\theta, \phi)$ and $\dot{\phi}^{\alpha}_{Rl}(r)Y_L(\theta, \phi) \equiv (\dot{\phi}_{Rl}(r) + o^{\alpha}\phi_{Rl}(r))Y_L(\theta, \phi)$, respectively. Here $\phi_{Rl}(r)$ and $\dot{\phi}_{Rl}(r)$ denote the solutions of the radial Schrödinger equation and its energy derivative. We denote these basis functions together as $\phi_{Ra}(\boldsymbol{r})$ hereafter. (o^{α} was introduced in the LMTO-ASA method so that the logarithmic derivatives of $\dot{\phi}^{\alpha}_{Rl}(r)$ at $r = \bar{R}$ agree with those of $J^0_{Rl}(r) - \alpha K^0_{Rl}(r)$, where α is the screening parameter, and J^0 and K^0 are the regular and irregular solutions of the Laplace equation, respectively. See reference [8].) As a result, $\psi^{kj}(\boldsymbol{r}, R)$ can be expanded as

$$\psi^{kj}(\boldsymbol{r}, R) = \sum_a A^{kj}_{Ra}\phi_{Ra}(\boldsymbol{r}). \tag{1}$$

We have two independent basis functions, the ϕ-basis and the $\dot{\phi}$-basis, in each of the RL-channels in the expansion. From these eigenfunctions (and eigenvalues), we can calculate the screened Coulomb interaction $W(\boldsymbol{r}R, \boldsymbol{r}'R', \omega)$ in the RPA. Expressed symbolically, it is

$$W = v(1 - P^0 v)^{-1} \tag{2}$$

where

$$P^0(\boldsymbol{r}R, \boldsymbol{r}'R', \omega) = \sum_{abcd} \phi_{Ra}(\boldsymbol{r})\phi_{Rb}(\boldsymbol{r})P^0(Rab, R'cd, \omega)\phi_{R'c}(\boldsymbol{r}')\phi_{R'd}(\boldsymbol{r}'). \tag{3}$$

Here P^0 is the non-interacting dielectric function constructed from the eigenfunctions and eigenvalues, and v is the bare Coulomb interaction.

The $\phi_{Ra}(\boldsymbol{r})$ are classified into two sets: an internal part I, and an external part E. For example, we can identify I as the ϕ-basis for 3d, and E as the other ϕ-basis and the $\dot{\phi}$-basis.

The electron density is expanded as

$$\hat{n}(\boldsymbol{r}R) = \sum_{ab} \hat{n}_{Rab}\phi_{Ra}(\boldsymbol{r})\phi_{Rb}(\boldsymbol{r})$$

and we can define a set of the internal parts of the coefficients as $I_n \equiv \{\hat{n}_{Rab}|\ Ra \in I$ and $Rb \in I\}$ and a set of the external parts as $E_n \equiv \{\hat{n}_{Rab}|Ra \in E$ or $Rb \in E\}$. The effective interaction $\tilde{W}(\boldsymbol{r}R, \boldsymbol{r}'R', \omega)$ for the internal degree of freedom corresponding to I is defined as a renormalized interaction; we take into account the contribution of the external part $\hat{n}_{Rab} \in E_n$ as the polarizable medium evaluated in the RPA. As a result, we obtain $\tilde{W}$ as

$$\tilde{W} = v(1 - \tilde{P}^0 v)^{-1} \tag{4}$$

where $\tilde{P}^0$ is a dielectric function that is identical to P^0 defined in equation (3) except that we omit terms containing products $\phi_{Ra}(\boldsymbol{r})\phi_{Rb}(\boldsymbol{r})$ ($Ra \in I$ and $Rb \in I$) or $\phi_{R'c}(\boldsymbol{r}')\phi_{R'd}(\boldsymbol{r}')$ ($R'c \in I$ and $R'd \in I$). The internal part of the self-energy Σ_{I} can be calculated from the internal parts of the Green functions $I_{\mathrm{G}} \equiv \{G_{RaR'b}(\omega)|Ra \in I$ and $R'b \in I\}$ and the effective interaction

$$\tilde{W}(Rab, R'cd, \omega) \equiv \langle \phi_{Ra}(\boldsymbol{r})\phi_{Rb}(\boldsymbol{r})|\tilde{W}(\boldsymbol{r}R, \boldsymbol{r}'R', \omega)|\phi_{R'c}(\boldsymbol{r}')\phi_{R'd}(\boldsymbol{r}')\rangle.$$

We can obtain the total self-energy Σ by adding the other contributions to it. We refer to the method used to calculate $\tilde{W}$ in this way as the PRPA method.

We have carried out the calculations using the code originally due to Aryasetiawan and Gunnarson [9] within the LMTO-ASA [10]. v, P^0, W, and so on, are expanded in the product basis. The Brillouin zone summations in the calculations of polarizations P^0 and $\tilde{P}^0$ have been performed by the tetrahedron method [11], with a small imaginary part $\delta = 0.01$ Ryd to avoid poles at the energies corresponding to the hole–electron excitation, though the method allows us to set $\delta = 0$ Ryd. (δ is defined in equation (28) of reference [9].) The dependence of the results on δ will be examined later.

We calculate the on-site ($R = R'$) part of W and $\tilde{W}$ for Ni, Fe, and MnO (in the Mn AS) for antiferromagnetic type-II ordering with the ordinary primitive cells. The number of k-points used in the irreducible Brillouin zone is 35 for Ni and Fe, and 19 for MnO. The calculations using some super-cells are also performed for Fe and Ni. For the valence part of the LMTO basis, we use 4s4p3d4f for Ni and Fe, and use 4s4p3d for Mn and 2s2p3d for O in the case of MnO. We start from the eigenvalues and eigenfunctions for the potentials given by the scalar-relativistic self-consistent calculation within the LDA for Fe and Ni. For MnO we take a potential obtained by an optimized-effective-potential (OEP) method where we treated the exchange and RPA correlation in the framework of an inhomogeneous RPA calculation [12].

2. Ni and Fe

If we assume spherical (atomic) symmetry, the interactions W are specified by the three Racah parameters, $A(\omega)$, $B(\omega)$, and $C(\omega)$ [3]. They determine the two kinds of matrix

$$U(m, m', \omega) \equiv \langle mm'|W(\boldsymbol{r}R, \boldsymbol{r}'R, \omega)|m'm'\rangle$$

and

$$J(m, m', \omega) \equiv \langle mm'|W(\boldsymbol{r}R, \boldsymbol{r}'R, \omega)|m'm\rangle$$

where m denotes the 3d basis, and takes the forms xy, yz, zx, $x^2 - y^2$, and $3z^2 - r^2$. We also introduce U, J, $A(\omega)$, $B(\omega)$, and $C(\omega)$ for $\tilde{W}$ in a similar manner. Our calculation shows that the deviations from spherical symmetry for W and $\tilde{W}$ are small. For example, the difference between $U(xy, xy, \omega = 0)$ and $U(x^2 - y^2, x^2 - y^2, \omega = 0)$ is $\sim$2% for $\tilde{W}$.

We treat the ϕ-basis for 3d as the internal part I, and the other ϕ-basis and the $\dot{\phi}$-basis as the external part E. Then $\tilde{P}^0$ depends on how we define the two independent 3d basis functions ϕ and $\dot{\phi}$. There are two degrees of freedom, other than normalization, available for defining the two bases, which correspond to two parameters: the logarithmic derivative D_{3d} and the tight-binding screening parameter α_{3d} [8]. We use $\alpha_{3d} = 0.011$ as given by the LMTO-4 code [10], and use $D_{3d} = -3.0$. Because we use a value of D_{3d} that is independent of the spin, the spin dependence of $U(m, m', \omega)$ and $J(m, m', \omega)$ is rather small (less than $\sim$5%, as for the diagonal part) and we show spin-averaged values only.

Figure 1 shows the Racah parameters calculated in the RPA and in the PRPA up to $\omega = 1$ Ryd. The diagonal parts $U(m, m, \omega)$ $(=A + 4B + 3C)$ are also shown. In the RPA, the diagonal parts show a rather large ω-dependence and their imaginary parts are larger than the real part at $\omega \gtrsim 0.2$ Ryd. The ω-dependence arises mainly from A. The real parts of A, B, and C in the PRPA show rather small ω-dependence. The imaginary parts are larger than half the real parts at $\omega \gtrsim 0.7$ Ryd though they are much smaller than those of the RPA results. Because of the small ω-dependence and the small imaginary parts of A, B, and C in the PRPA, we expect to be able to calculate the on-site 3d part of the self-energy, by using a local approximation, from their static values and the on-site 3d ϕ-basis part of the Green function. Such a treatment is apparently free from the problem of double counting of the polarization

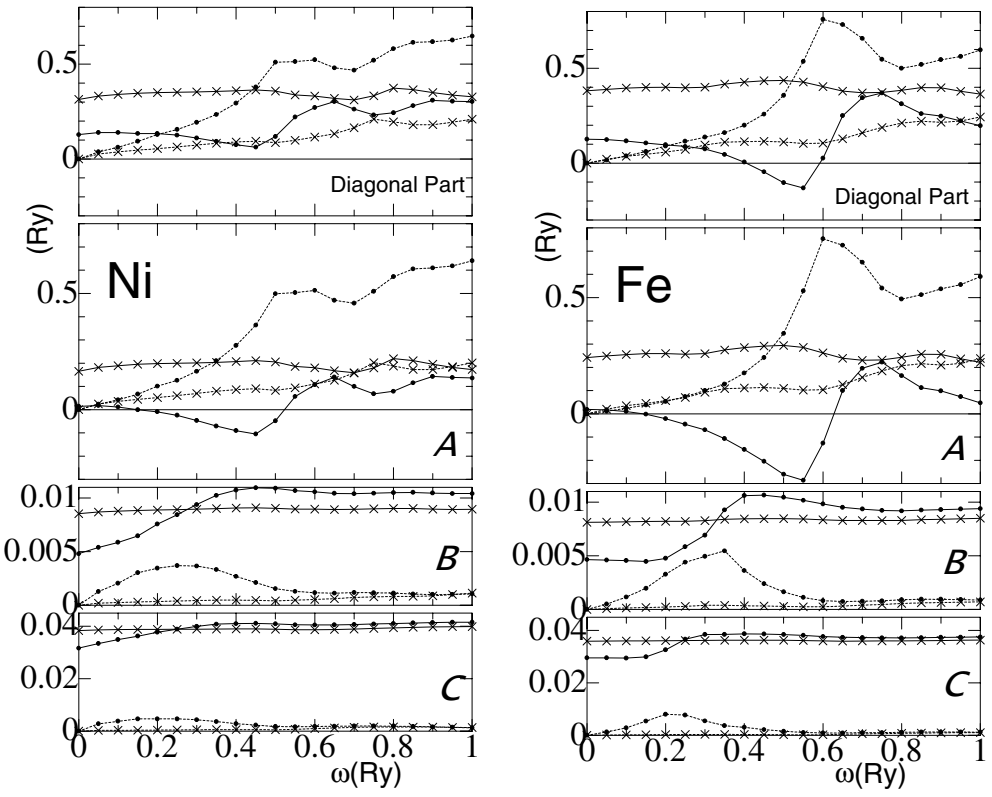

Figure 1. The calculated Racah parameters A, B, and C for Ni (a) and Fe (b). Dots are for W in the RPA and crosses are for $\tilde{W}$ in the PRPA. The diagonal part is defined as $A + 4B + 3C$. Solid lines and broken lines denote real parts and imaginary parts, respectively.

for screening due to the 3d electrons. We give some further checks below.

In figure 2, we compare A in the case of (a) 35 k-points with a 4s4p3d4f basis as shown in figure 1 with the cases of (b) 35 k-points with a 4s4p3d basis and (c) 72 k-points with a 4s4p3d basis. It demonstrates that the convergence with respect to the number of k-points seems reasonable. A^{RPA} for the 4s3p3d case and that for 4s3p3d4f show good agreement at $\omega \sim 0$ Ryd but the agreement gradually becomes poor for larger ω, especially at $\omega \gtrsim 0.5$ Ryd. The agreement is consistent with the well known fact that the static ground-state densities are well described by a 4s3p3d basis. On the other hand, the real part of $A^{\mathrm{PRPA}}(\omega = 0$ Ryd) for 4s3p3d4f is ∼0.05 Ryd smaller than that for 4s3p3d. We also see a larger difference for larger ω in the imaginary part. This is reasonable because some weight of the PDOS for 3d in the 4s3p3d case shifts to that for 4f in the 4s3p3d4f case. This means we have to project out a smaller part of P^0 in the case of 4s3p3d4f than in the case of 4s3p3d. This results in larger screening and gives a smaller $\tilde{W}$. In figure 3, we show the dependence on the imaginary part δ. The case of $\delta = 10^{-1}$ Ryd gives substantially flattened structures. On the other hand, the case of $\delta = 10^{-2}$ Ryd is little different from the case with $\delta = 10^{-8}$ Ryd. The RPA value of the diagonal part of Ni (0.13 Ryd) shown in figure 1 is a little different from the value (0.16 Ryd) obtained by Springer and Aryasetiawan [7]. This discrepancy could be a result of the flattening.

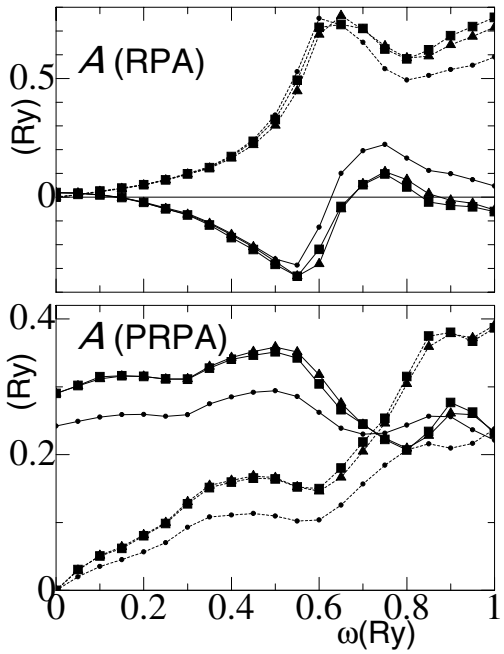

Figure 2. Dependences of the A-parameters for Fe on the number of k-points and the angular-momentum cut-off. We show A for W in the RPA and A for $\tilde{W}$ in the PRPA. Dots denote the case of 35 k-points with a 4s4p3d4f basis. Triangles and squares denote the cases of 35 k-points and 72 k-points, respectively, with a 4s4p3d basis. Solid lines and broken lines denote real parts and imaginary parts, respectively.

The 3d part of the eigenfunctions should be reproduced well by just the internal part of the Green function I_{G}—that is, the ϕ-basis part. This is necessary for a good description of the correlation effects for 3d and is crucial in calculating the self-energy from I_{G} and $\tilde{W}$. In figure 4, the hatched region denotes the 3d PDOS—that is, the DOS for the 3d eigenfunctions

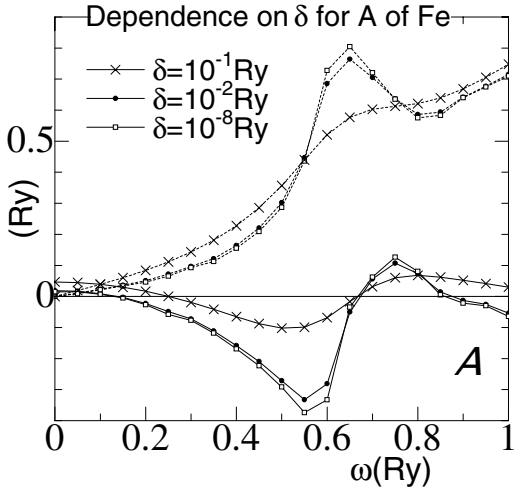

Figure 3. The dependence of the A-parameter for Fe (for W in the RPA) on the imaginary part δ which is used in the tetrahedron method for the calculation of the polarization functions P^0 and $\tilde{P}^0$. Solid lines and broken lines denote real parts and imaginary parts, respectively.

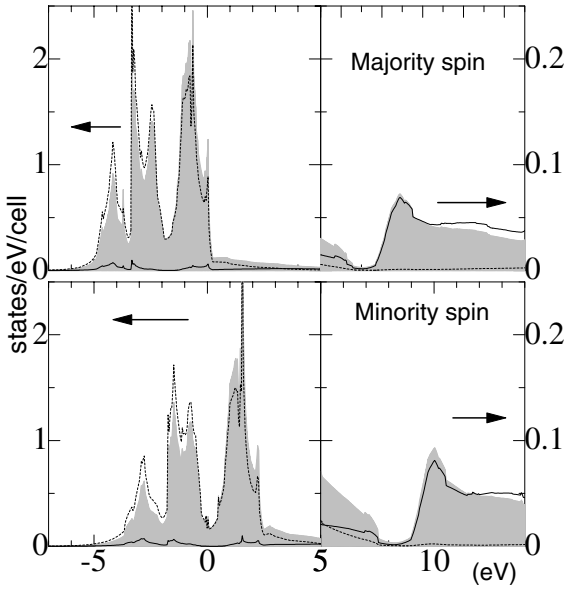

Figure 4. Hatched regions show the PDOS of Fe 3d. Broken lines show its contributions from the ϕ-basis for 3d. Solid lines show the differences of the two kinds of 3d part of the eigenfunctions (see the text). We set the Fermi energy at 0 eV.

$\psi_d^{kj}(\boldsymbol{r})$—and the broken lines denote the DOS for the 3d eigenfunctions without the $\dot{\phi}$-basis, $\tilde{\psi}_d^{kj}(\boldsymbol{r})$. The solid lines show the difference

$$\Delta_d^2(\omega) = \sum_{kj} \int_R \mathrm{d}^3 r \; |\psi_d^{kj}(\boldsymbol{r}) - \tilde{\psi}_d^{kj}(\boldsymbol{r})|^2 \delta(\omega - \omega^{kj})$$

which equals the product of the parts of $\dot{\phi}$ in the calculation of the PDOS for 3d. Our calculation

shows that the difference $\Delta_d^2(\omega)$ is satisfactorily small, and the PDOS for $\tilde{\psi}_d^{kj}(\boldsymbol{r})$ shows a good agreement with that for $\psi_d^{kj}(\boldsymbol{r})$ for ω, in which the main peaks for 3d are included. Admittedly, we still have some disagreement, especially concerning the weight of unoccupied states for majority spin above the Fermi energy. In figure 5, we show the case of $D_{3d} = -2.0$ to illustrate the effects of changes in the basis functions. For B and C, the difference is smaller than in the case of A (e.g. the real part of B and C at $D_{3d} = -2.0$ obtained within the PRPA is $\sim$2% smaller than those for $D_{3d} = -3.0$).

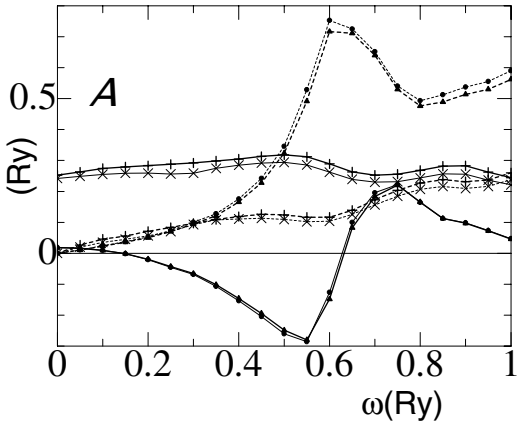

Figure 5. The A-parameters for Fe for different values of D_{3d}. We show A for W in the RPA and A for $\tilde{W}$ in the PRPA. Triangles and dots denote W for $D_{3d} = -2.0$ and $D_{3d} = -3.0$, respectively. + and $\times$ denote $\tilde{W}$ for $D_{3d} = -2.0$ and $D_{3d} = -3.0$, respectively. Solid lines and broken lines denote real parts and imaginary parts, respectively.

In figure 6, we show a screened Coulomb interaction $\bar{W}$ which is calculated by an on-site-only RPA calculation with $\tilde{W}$ and the on-site 3d dielectric functions P^{3d}. Here P^{3d} is calculated from the 3d ϕ-basis part of the on-site Green function $\{G_{Ra,Rb}|a, b \in (3d\ \phi\text{-basis})\}$. This RPA calculation was done in the real-space representation. This $\bar{W}$ is equal to that from a RPA calculation with the dielectric function $\tilde{P}^0 = \tilde{P}^0 + P^{3d}$. Figure 6 shows that $\bar{W}$ is rather

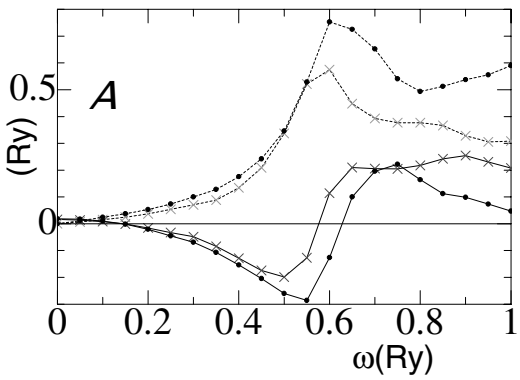

Figure 6. The A-parameters for Fe. The $\times$ denote the A-parameters calculated by an on-site-only RPA calculation with the on-site 3d Green function and the on-site $\tilde{W}$. Dots denote W in the RPA, shown for reference. Solid lines and broken lines denote real parts and imaginary parts, respectively.

close to $\tilde{W}$ though there are some differences for larger ω. This means that the difference $P^0 - \tilde{P}^0$, which is the polarization between I_n and E_n, gives relatively small effects. This is one justification for our division into contributions I_n and E_n and treating E_n as a polarizable medium. If $\bar{W}$ differed substantially from $\tilde{W}$, it would mean that the connection between I_n and E_n was too close, and such a treatment might not be justifiable.

The calculations that have been described were carried out using the primitive unit cell. However, many theoretical calculations like those in reference [2] are based on impurity-like treatments. For such treatments, we have to calculate the effective interaction in the impurity-like configuration—that is, we only identify the 3d ϕ-basis in the central AS (a site treated as an impurity) as the internal part I. Because too much computational effort is needed for large super-cells, we chose a super-cell of minimum size. In the case of Fe with fcc structure, our super-cell contains two Fe atoms, Fe1 and Fe2, and we just identify the ϕ-basis for 3d in Fe1 as the internal part. Figure 7 shows that the difference from the case with the primitive cell is rather small. We have made similar calculations for Ni, and we obtained similar results. This shows that we do not need the impurity-like configuration for the calculation of $\tilde{W}$. The polarization effect of 3d electrons on the other sites should be negligible.

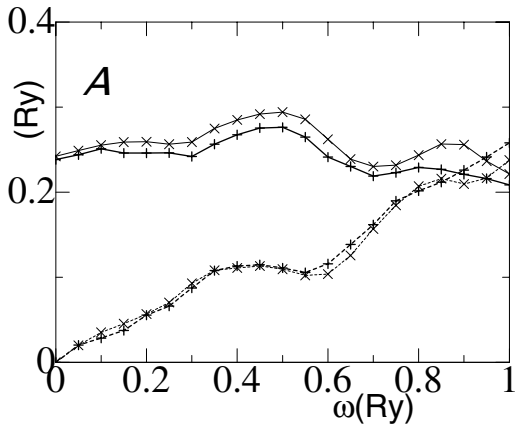

Figure 7. The A-parameters for $\tilde{W}$ in the PRPA given by a super-cell calculation for Fe. The + denote the case with the super-cell and the × denote the case with the primitive cell, shown for reference. Solid lines and broken lines denote real parts and imaginary parts, respectively.

3. MnO

The lattice constant used is 10.26 au, and we set the ASA radii $\bar{R}$ for Mn and O as 2.923 au and 2.2 au, respectively. Within the ASA, we can define the Mn 3d PDOS for majority and minority spins in each Mn AS. In figure 8, we show them calculated by an OEP method [12]. The correspondence of the 3d PDOS to experiments seems good, though we note that the minimum band gap 2.3 eV is smaller than the experimental value of 3.7 eV. We have to choose the internal part I so as to reproduce the 3d PDOS well, as was discussed for the Fe case. At first, we tried a similar analysis to that used for the Fe case, in order to select the ϕ-basis for 3d in such a way that the ϕ-basis part of the Green function will almost give the 3d PDOS. However, the analysis shows that it is difficult to choose a ϕ-basis which reproduces the wide energy range of the 3d PDOS for occupied and unoccupied bands. This is because the behaviour of the 3d radial function as a function of ϵ_{3d} (ϵ_{3d} is the energy appearing in the 3d radial Schrödinger

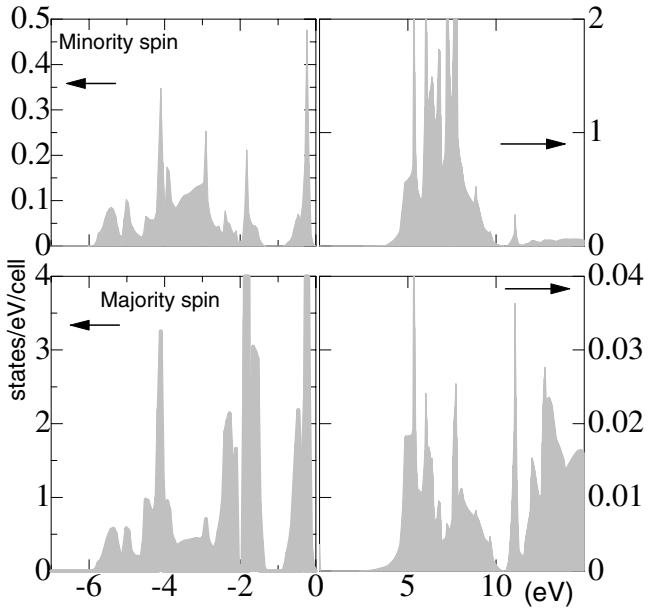

Figure 8. The 3d PDOS in a Mn atomic sphere for each spin for MnO calculated by an optimized-effective-potential method [12]. The upper two panels are for the minority spin in the Mn atomic sphere and the lower two are for the majority spin. The zero of the x-axis denotes the top of the valence bands.

equation measured from the Fermi energy) changes so much within the range. Therefore we decided here to treat all the 3d channels of the radial basis—that is, the ϕ- and $\dot{\phi}$-bases for 3d for the Mn AS are identified as the internal part I. Correspondingly, I_{G} contains all the 3d channels of the Green functions expanded in these bases.

In figure 9, we show the diagonal parts of W and $\tilde{W}$ for occupied states and unoccupied states for each spin. We choose $\epsilon_{3\mathrm{d}} = -3.0$ eV for occupied states and $\epsilon_{3\mathrm{d}} = 7.0$ eV for unoccupied states. The smallness of the diagonal parts for the minority-spin occupied states is due to the differences of the 3d radial functions. $D_{3\mathrm{d}}$ for the minority-spin occupied, the majority-spin occupied, the minority-spin unoccupied, and the majority-spin unoccupied states are +1.24, −1.56, −4.90, and +1.53, respectively (the radial function of the majority-spin unoccupied states has a node). The radial functions of the minority-spin occupied states are rather delocalized. Corresponding to this delocalized character, the interactions W and $\tilde{W}$ between the bases of the minority-spin occupied states and of the other states are also small, though they give similar energy dependences; the value of $\tilde{W}$ varies from ∼0.45 Ryd (at $\omega = 0$) to ∼0.25 Ryd (at $\omega = 1$ Ryd).

We have calculated the effective interactions of 3d electrons for Ni, Fe, and MnO. As for Ni and Fe, we obtain the Racah parameters A, B, and C, which give a rather flat energy dependence. This might provide some justification for using ω-independent values in model calculations. In the case of MnO, our analysis shows that it might be necessary to include the $\dot{\phi}$-basis for 3d in addition to the ϕ-basis for 3d as the internal part I. Then the effective interaction is substantially dependent on the spins and $\epsilon_{3\mathrm{d}}$, which specify the 3d basis functions. The interaction $\tilde{W}$ depends on the way in which we choose the internal part I, and so we should calculate the local part of the self-energy Σ_{I} from I_{G} and $\tilde{W}$ which might be determined in the way that we proposed.

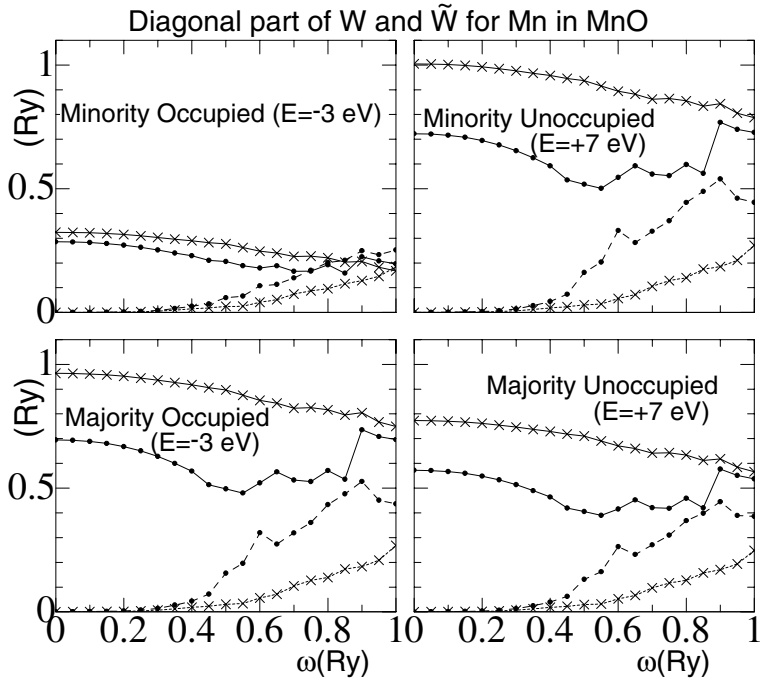

Figure 9. The calculated diagonal parts of W and of $\tilde{W}$ for Mn in MnO. Dots and $\times$ denote W in the RPA and $\tilde{W}$ in the PRPA, respectively. Solid lines and broken lines denote real parts and imaginary parts, respectively.

Acknowledgments

I thank F Aryasetiawan for his GW-program and for stimulating discussions, and M van Schilfgaarde, T A Paxton, O Jepsen, and O K Andersen for their TB-LMTO program. I also thank H Akai for discussions and for a critical reading of the manuscript.

References

[1] Springer M, Aryasetiawan F and Karlsson K 1998 *Phys. Rev. Lett.* **80** 2389
[2] Lægsgaard J and Svane A 1997 *Phys. Rev.* B **55** 4138
[3] Igarashi J, Unger P, Hirai K and Flude P 1994 *Phys. Rev.* B **49** 16 181
Takahashi M and Igarashi J 1996 *Phys. Rev.* B **54** 13 566
[4] Anisimov V I, Aryasetiawan F and Lichtenstein A I 1997 *J. Phys.: Condens. Matter* **9** 767
[5] Gunnarson O, Andersen O K, Jepsen O and Zaanen J 1989 *Phys. Rev.* B **39** 1708
[6] Hedin L and Lundqvist S 1969 *Solid State Physics* vol 23, ed H Ehrenreich, F Seitz and D Turnbull (New York: Academic) p 1
[7] Springer M and Aryasetiawan F 1998 *Phys. Rev.* B **57** 4364
[8] Andersen O K, Pawloska Z and Jepsen O 1986 *Phys. Rev.* B **34** 5253
[9] Aryasetiawan F and Gunnarson O 1994 *Phys. Rev.* B **49** 16 214
[10] van Schilfgaarde M, Paxton T A, Jepsen O and Andersen O K 1992 *The TB-LMTO Program Version 4* Max-Planck-Institut für Festkörperforschung, Federal Republic of Germany
[11] Rath J and Freeman A J 1975 *Phys. Rev.* B **11** 2109
[12] Kotani T 1998 *J. Phys.: Condens. Matter* **10** 9241